Check for updates

Au(ɪ)-, Ag(ɪ)-, and Pd(ɪɪ)-coordination-driven diverse self-assembly of an N-heterocyclic carbene-based amphiphile†

Toshiaki Taira, [iD] *[a] Takaya Yanagimoto,[b] Kenichi Sakai, [iD] [b] Hideki Sakai[b] and Tomohiro Imura‡[a]

Au(ɪ)-, Ag(ɪ)-, and Pd(ɪɪ)-coordination-driven diverse self-assembly of an N-heterocyclic carbene (NHC)-based amphiphile was demonstrated herein. The transition metals had significant effects over the whole system, setting the self-assembly direction of the NHC-based amphiphile. More specifically, Au(ɪ)- and Ag(ɪ)-coordination to the NHC-based amphiphile promoted the formation of spherical and hexagonal structures, while Pd(ɪɪ)-coordination promoted the formation of cylindrical and lamellar structures.

Introduction

Self-assembly based on the principles of supramolecular chemistry affords a range of versatile nanostructures.[1] Recent developments in materials science based on the advanced concept of nanoarchitectonics have allowed for the bottom-up synthesis of functional nanomaterials *via* the self-assembly of building blocks into hierarchic structures with atomic level precision. The resultant structures have potential for applications in catalysis and the development of electric materials.[2] The incorporation of transition metals into building blocks can impart diverse properties due to their varied electronic configurations and bonding patterns. Indeed, in nature, enzymes present three-dimensional structures, and transition metals are often located in the pockets of the active sites of enzymes. However, the regulation of transition metals within nanostructures *via* the self-assembly of building blocks remains a challenge in materials science due to the subtle balance between metal coordination and self-assembly.

Metallosurfactants (MSs) are a new class of building blocks, in which ligand moieties in the surfactant framework bind to various transition metals.[3] Since transition metals are incorporated within the surfactants, they can form various self-assembled structures with metallic interfaces, such as micelles, lyotropic liquid crystals, and vesicles. However, MSs typically consist of a transition metal cation bound to an anionic surfactant; therefore, transition metal leaching occurs

easily in water due to the weak ionic bonds. To overcome such limitations, our group focused on N-heterocyclic carbenes (NHCs), which are derived from imidazolium salts, as a new class of MS frameworks. Due to their electron-rich nature and σ-donating capability, NHCs form robust metal–carbene bonds with a broad spectrum of metals, even under aqueous conditions.[4] Previously, we reported the synthesis of an NHC-based amphiphile bearing an octaethyleneglycol monomethylether and a dodecyl chain.[5] Although its structure was similar to that of commonly used non-ionic surfactants, the amphiphile exhibited the advanced function of a ligand to ultimately afford Pd(ɪɪ)- and Au(ɪ)-coordinated surfactants (*i.e.*, Pd-MS and Au-MS), as shown in Fig. 1.[6,7] We found that their surface
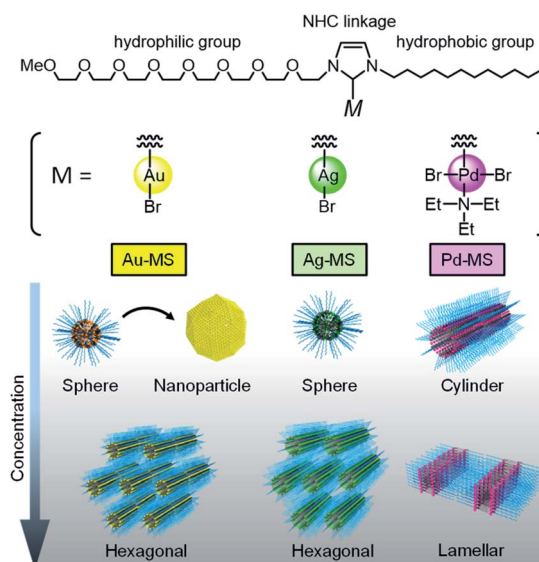
[a]National Institute of Advanced Industrial Science and Technology (AIST), Central 5-2, 1-1 Higashi, Tsukuba, Ibaraki 305-8565, Japan. E-mail: t-taira@aist.go.jp

[b]Faculty of Science and Technology, Tokyo University of Science, 2641 Yamazaki, Noda, Chiba 278-8510, Japan

‡ Deceased author (December 5, 2020).

Fig. 1 Metallosurfactants (MSs) and their self-assembled structures.

properties were significantly influenced by the transition metal employed, despite using the same NHC amphiphile.

Motivated by the capability to bond a broad spectrum of metals, we herein report the synthesis of the corresponding Ag(I)-coordinated surfactant (Ag-MS) using our previously reported NHC-based amphiphile. A systematic investigation was then conducted into the self-assembled structures of the Ag(I)-, Au(I)-, and Pd(II)-based systems.

Experimental

Materials

The NHC-based amphiphile (MS precursor), Pd-MS, and Au-MS were synthesized according to literature methods.[5,6] Ag_2O was purchased from Tokyo Chemical Industry, Co., Ltd. Acetone (99.0%), dichloromethane (99.5%), methanol (99.5%), chloroform (99.0%) and tetrahydrofuran (THF) were purchased from Fujifilm Wako Pure Chemical Industries, Ltd. and were used as received.

Synthesis and characterization

^{1}H-NMR spectra were recorded on a Bruker NMR spectrometer (Avance 400, Bruker Biospin Co., Inc., USA) operated at 400 MHz. ^{13}C-NMR spectra were recorded on the same instrument operated at 100 MHz. All the NMR spectra were recorded in $CDCl_3$. Both the ^{1}H-NMR and ^{13}C-NMR spectra were calibrated using tetramethylsilane as an internal reference. Elemental analyses were carried out using a Flash 2000 instrument (Thermo Fisher Scientific Inc., USA). Matrix-assisted laser desorption-ionization time-of-flight mass spectroscopy (MALDI-TOF-MS) was conducted on an autoflex speed TOF/TOF MS (Bruker Daltonics Inc.).

The MS precursor (1.00 g, 1.46 mmol), Ag_2O (0.17 g, 0.73 mmol), and dichloromethane (30 mL) were placed in a vial tube equipped with a magnetic stir bar. The mixture was stirred for 2 h at ambient temperature. The solution was filtered through Celite and a polytetrafluoroethylene (PTFE) filter (pore size: 0.45 μm). The solvent was evaporated under reduced pressure and Ag-MS was obtained as a pale-yellow oil (1.1 g, 1.39 mmol, 95%). ^{1}H NMR (400 MHz, $CDCl_3$) δ 7.21 (s, 1H), 6.93 (s, 1H), 4.26 (t, J = 4.0 Hz, 2H), 4.05 (t, J = 6.0 Hz, 2H), 3.76 (t, J = 4.0 Hz, 2H), 3.48–3.74 (28H), 3.35 (s, 3H), 1.77 (t, J = 8.0 Hz, 2H), 1.15–1.40 (18H), 0.85 (t, J = 8.0 Hz, 3H); ^{13}C NMR (100 MHz, $CDCl_3$) δ 180.3, 122.4, 120.3, 71.9, 70.7, 70.5, 70.4 (2C), 58.9, 52.0, 51.7, 31.8, 31.4, 29.5, 29.4 (2C), 29.2, 29.1, 26.5, 22.6, 14.2; MALDI-TOF-MS analysis of $C_{32}H_{62}AgBrN_2O_8$: calculated m/z = 709.4; observed m/z = 709.5 $[M–Br]^+$. Anal. calcd for $C_{32}H_{62}AgBrN_2O_8$: C, 48.61; H, 7.90; N, 3.54. Found: C, 48.67; H, 7.93; N, 3.57.

Surface tension measurements

The surface tension measurements of the surfactant solutions were conducted by the Wilhelmy plate method at 25 °C using a DY-500 surface tension meter (Kyowa Kaimen Kagaku Co.), whose accuracy was intermittently checked with ultrapure water. The Pt plate was cleaned by flame cleaning, and all glassware was rinsed sequentially with tap water and ultrapure water. The critical micelle concentration (CMC) and surface tension at the CMC (γ_{CMC}) were determined from the curve of the break point of surface tension *versus* the logarithm of the concentration.

UV-vis spectroscopy

Au-MS and Ag-MS aqueous solutions (0.1 mM) were prepared in vial tubes. The aurophilic interactions were monitored using a UV-vis spectrometer (V-530, JASCO). Time-dependent UV-vis spectra of Au-MS were recorded at several time intervals during the first 300 min. UV-vis spectrum of Ag-MS was recorded 1180 min after dissolving Ag-MS in water.

Dynamic light scattering (DLS)

The size distributions of the assemblies of MSs were measured using a DLS instrument (DLS-7000, Otsuka Electronics Co., Japan) using a 488 nm Ar laser (75 mW) as a light source (25 °C). The time-dependent correlation function of the scattered light intensity was measured at a scattering angle of 90°. The particle size distributions were determined using the software provided with the instrument. In this study, the autocorrelation function was analysed using the histogram method.

Transmission electron microscopy (TEM)

The solutions of Au-MS and Ag-MS were dropped on a glow-discharged copper grid (200 mesh) coated with C (Excel support film, Nisshin EM Co.). The solution was blotted using a filter paper, and the grid was thoroughly dried. Images of Au-MS and Ag-MS were acquired on an H-7650 transmission electron microscope (Hitachi High-Technologies) and JEM-1400Flash electron microscope (JEOL), respectively.

Small angle X-ray scattering (SAXS)

To prepare MS/water samples, ultrapure water was added to sample tubes containing Au-MS, Ag-MS, or Pd-MS. The mixtures were then vigorously mixed using a vortex mixer. Before measuring, the samples were kept at room temperature for several hours. X-ray scattering data were then recoded on a SAXSess camera (Anton Paar Co., Ltd., Austria) using a system equipped with a W3830 sealed glass bulb X-ray source (PANalytical Co., Ltd., Netherland, Cu-Kα (λ = 0.154 nm)). The diffraction pattern was recorded with an imaging plate, and the exposure time was 20 min for each sample. The scattering vector q was calculated using $q = (4\pi/\lambda)\sin\theta$, where 2θ is the scattering angle. Indirect Fourier Transformation (IFT) of an aqueous solution of Pd-MS (10 mM) was carried out according to reference procedures.[8–10]

Results and discussion

Synthesis and characterization

The synthesis of Ag-MS was achieved by the reaction of the MS precursor with Ag_2O in dichloromethane at ambient temperature. Ag-MS was obtained as a pale-yellow oil in 95% yield. The ^{1}H NMR spectrum of Ag-MS was found to be similar to that of

Au-MS, with resonances corresponding to the protons of the imidazole backbone being observed at 7.20 and 6.90 ppm, respectively, for Au-MS and 7.21 and 6.93 ppm, respectively, for Ag-MS (Fig. S1 and S3, ESI†). In the ^{13}C NMR spectra, the chemical shifts for the carbenoid carbons were found at 173.6 ppm (Fig. S2 and S4, ESI†) for Au-MS and 180.3 ppm for Ag-MS.[11] Notably, the carbenoid carbon of Ag-MS appeared as singlet. Since Ag has two almost equally abundant nuclei with spin 1/2, the carbenoid carbon of Ag-MS should form a doublet of doublets. This anomaly indicates that Ag-MS exhibits fluxional behaviour in solution, such as ligand exchange, which occurs more rapidly than the NMR time scale (Fig. S5, ESI†).[12]

Surface properties

To reveal the diverse structure–property relationship for the MSs, their surface properties were confirmed using the Wilhelmy plate method, as outlined in Table 1. The CMCs of the MSs are lower than that of the NHC-based amphiphile (3.9×10^{-3} M),[5] indicating that metal coordination promoted self-assembly in water. The CMC of Au-MS (1.3×10^{-5} M)[7] was found to be one order of magnitude lower than that of Ag-MS (7.3×10^{-4} M), even though they consist of the same NHC and bromide ligands (Fig. S6, ESI†). In addition, the CMC of Pd-MS (1.4×10^{-4} M),[6] bearing triethylamine as an additional hydrophobic ligand, was similar to that of Ag-MS, thereby suggesting the distinctive role of Au(I). On this account, UV-vis spectroscopic measurements were performed for Au-MS. An aqueous solution of Au-MS (0.1 mM) showed absorption peaks at 224, 248, and 325 nm, respectively (Fig. S7, ESI†). The peak at 535 nm originated from the surface plasmon resonance (SPR) of gold nanoparticles (AuNPs) (*vide infra*). These absorption peaks were not observed when Ag-MS dissolved in water at the same concentration. The time-dependent absorption spectral change of Au-MS showed that the intensity of the absorption at 248 nm decreased in the spectra, accompanied with the increasing of absorptions of 224 and 325 nm, respectively (Fig. S8, ESI†). According to reference to the previous literature,[13] the spectral change can be attributed to the proximity of Au(I) atoms to the neighboring molecules. Thus, we assumed that aurophilic interactions such as Au(I)–Au(I) interactions promote self-assembly at the air/water interface, which results in the lowest CMC value of Au-MS.[14,15] In addition, the γ_{CMC} of Au-MS (44.9 mN m^{-1}) was higher than those of Ag-MS (29.6 mN m^{-1}) and Pd-MS (36.7 mN m^{-1}). Therefore, the alignment of the Au atom in Au-MS at the air/water interface may

hamper the disruption of the hydrogen bonds present in water, resulting in the γ_{CMC} of Au-MS being higher than those of Ag-MS and Pd-MS.[7]

Metal-dependent self-assembly

The metal-dependent self-assembly behaviour of the MSs was also investigated. Fig. 2(a) shows the time variation in the surface tension of the aqueous solution of Ag-MS (1 mM), which decreased gradually from 42.0 mM m^{-1} (immediately after the dissolution of Ag-MS) to a constant value of ~30.0 mN m^{-1} after 60 min. This behaviour could be attributed to the adsorption equilibrium of Ag-MS at the air/water interface. In contrast to Ag-MS, the surface tension of an aqueous solution of Au-MS (1 mM) gradually increased from 35.5 mN m^{-1} (upon the dissolution of Au-MS) to a constant value of 41.5 mN m^{-1} after 120 min (Fig. 2(b)). The adsorption equilibrium of Pd-MS at the
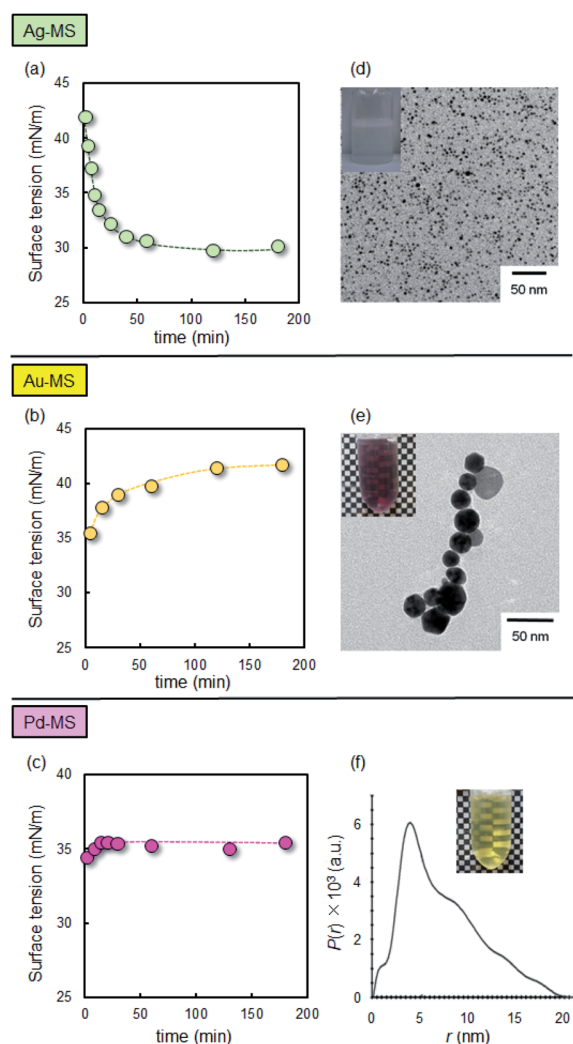

Fig. 2 Self-assembly behaviour of the MSs. Time-dependent surface tension measurements of water at 25 °C (a) Ag-MS (1 mM), (b) Au-MS (1 mM), and (c) Pd-MS (1 mM). (d) TEM image of Ag-MS (1 mM). (e) TEM image of the AuNPs obtained from Au-MS (1 mM). (f) The pair-distance distribution functions (PDDF) for the Pd-MS micellar solution (10 mM) at 25 °C The insets in (d–f) show photographic images of the solutions.

Table 1 Values of the critical micelle concentration (CMC), surface tension at the CMC (γ_{CMC}), and averaged hydrodynamic diameter of the micelle (d)

MS	CMC (M)	γ_{CMC} (mN m^{-1})	d^c (nm)
Au-MS	1.3×10^{-5a}	44.9^a	$5.7 \pm 1.1^{a,d}$
Ag-MS	7.3×10^{-4}	29.6	5.1 ± 0.9
Pd-MS	1.4×10^{-4b}	36.7^b	25.8 ± 5.6^b

[a] Data are taken from ref. 7. [b] Data are taken from ref. 6. [c] The averaged hydrodynamic diameters of the micelles were determined by DLS. [d] DLS data after removal of the AuNPs by filtration (PVDF, 0.45 μm pore size).

air/water interface was different than those of Ag-MS and Au-MS. The surface tension of water reached a constant value of $\sim$35.4 mN m^{-1} after 14 min.

The self-assembled structures of the MSs were also confirmed. In the case of Ag-MS, TEM observations of an aqueous solution of Ag-MS (1 mM) showed spherical micelles, as shown in Fig. 2(d). DLS measurements of the colourless solution also support the presence of the spherical micelles, whose averaged diameter was estimated to be 5.1 $\pm$ 0.9 nm (Table 1 and Fig. S9, ESI†). In addition, the TEM image gave excellent contrast without the requirement of heavy-metal stains, thereby indicating that the surfaces of the spherical micelles were covered with Ag(ı). In contrast to that of Ag-MS, a 1 mM solution of Au-MS exhibited a colour change from colourless to pink, which originated from SPR, as shown in the inset of Fig. 2(e).[16] A TEM image of the resulting solution showed large aggregates, thereby confirming the formation of AuNPs. Removal of the AuNPs by filtration (PVDF, 0.45 μm) provided a colourless solution, which was found by DLS measurements to contain spherical micelles with diameters of approximately 5.7 $\pm$ 1.1 nm (Table 1). Although Au-MS promoted AuNP formation, it exhibited the lowest CMC value among the various MSs (Table 1). These results indicate that Au-MS mainly adsorbs at the air/water interface *via* van der Waals interactions. In this case, Au(ı)–Au(ı) interactions promote integrated Au(ı) clusters at the air/water interface, resulting in their partial translation into AuNPs.[17] The averaged diameter of the spherical micelles of Ag-MS and Au-MS were similar to that of the NHC-based amphiphile (3.0 $\pm$ 0.5 nm) while the corresponding value for Pd-MS was significantly larger (25.8 $\pm$ 5.6 nm).[6] To study the geometry of the micelle, a SAXS measurement was performed on a 10 mM Pd-MS solution. The decay of $I(q)$ in the low q region suggests that the aggregates are not spherical micelles (Fig. S10, ESI†). Thus, to analyse the SAXS data, we employed the IFT method without considering any interparticle interactions. As shown in Fig. 2(f), the scattering intensity is related to the pair distribution function (PDDF) curve, which exhibits an asymmetry in the shape of the $p(r)$ curve, as anticipated by a pronounced peak in the low-r side and an elongated tail to the higher-r side. Indeed, this curve is typical of cylindrical micelles.[18] In addition, the value of r at which $p(r)$ reaches zero can be used as an estimation of the maximum dimension (D_{max}), *i.e.*, 20 nm. The cross-sectional diameter was estimated to be 5 nm, based the inflection point on the slightly higher r-side of the maximum in the curve. Furthermore, D_{max} agreed with the average size of Pd-MS, as determined by DLS. These results suggest that spontaneous curvature of Pd-MS was different from that of Au-MS and Ag-MS, as coordination of triethylamine to Pd(ıı) at the *trans* position led to increased hydrophobicity and steric bulkiness. Consequently, Pd-MS can form cylindrical micelles.

Geometrical transformation

Following the successful Au(ı)-, Ag(ı)-, and Pd(ıı)-coordination-driven diverse self-assembly of the NHC-based amphiphile in dilute aqueous solutions, the geometrical transformation was examined at high concentrations (Fig. 3). Although the NHC-based amphiphile did not provide an anisotropic phase at any concentration, the Au(ı)- and Ag(ı)-coordinated MSs (Au-MS and Ag-MS) provided optically anisotropic phases. The difference between MSs and NHC-based amphiphile can be attributed to the shielding of electropositive repulsion of imidazolium moieties after metal coordination. The polarised optical microscopy image of Au-MS (60 wt%) showed a fan-like texture (inset of Fig. 3(a)), and the hexagonal structure (H$_1$) of Au-MS was confirmed by four major SAXS peaks in the typical peak ratio of 1 : $\sqrt{3}$: 2 : $\sqrt{7}$, as shown in Fig. 3(a). A similar result was observed for Ag-MS. Furthermore, the polarised optical microscopy image of Ag-MS (60 wt%) showed a smoky texture, which is also considered a characteristic texture of H$_1$ (inset in Fig. 3(b)). The SAXS peaks also gave the typical peak ratio of 1 : $\sqrt{3}$: 2 : $\sqrt{7}$ (Fig. 3(b)). The distance between the centres of the cylinders (a) of the hexagonal of Au-MS was estimated to be
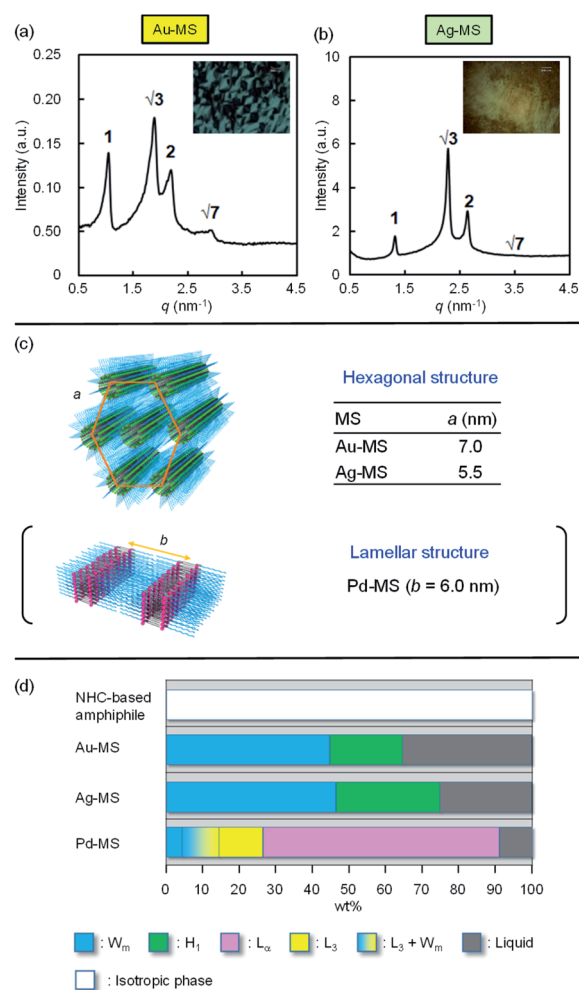

Fig. 3 Small angle X-ray scattering (SAXS) measurements of (a) Au-MS (60 wt%), and (b) Ag-MS (60 wt%). The insets show the optical polarised microscopy images of the samples. (c) Representation of the hexagonal structures of Au-MS and Ag-MS, and the lamellar structure of Pd-MS.[6] Centre-to-centre distances as obtained from the SAXS measurements are shown. (d) Two phase diagrams of the NHC-base amphiphile, Au-MS, Ag-MS, and Pd-MS[6] at 25 °C.

7.0 nm,[19] which is greater than the corresponding value for Ag-MS (5.5 nm), as shown in Fig. 3(c). The coordination of Pd(II) to the same NHC-based amphiphile led to the formation of a lamellar liquid crystal, whose lamellar d-spacing in the (100) plane was estimated to be 6.0 nm at the same concentration.[6] Fig. 3(d) summarises the concentration-dependent nature of the geometrical transformation of MSs at 25 °C. All the phases were identified by a combination of visual observations, polarised microscopy, and SAXS measurements (Fig. S11–S13, ESI†). On increasing the Au-MS concentration, the micellar solution became increasingly viscous. The phase transition from the isotropic micellar phase (W_m) to the anisotropic phase occurred above 46 wt%, where H_1 phases were observed. In the case of Ag-MS, W_m and H_1 phases were also found, while the region of H_1 was expanded. These self-assembled structures differed to that of Pd-MS, wherein the H_1 phase was not observed, and the L_3 (sponge) and L_α (lamellar) phases were detected. The formation of the lamellar structure suggests that the curvature of Pd-MS, bearing a triethylamine as an additional co-ligand, is considered close to zero. In contrast, Au-MS and Ag-MS, which did not contain triethylamine, exhibit positive curvatures, resulting in the formation of hexagonal structures.

Conclusions

We herein reported the diverse self-assembly of our previously reported NHC-based amphiphile that was driven by Au(I)-, Ag(I)-, and Pd(II)-coordination. We found that the identity of the transition metal has significant effect on the entire system, setting the self-assembly direction of the NHC-based amphiphile. More specifically, Au(I)- and Ag(I)-coordination to the NHC-based amphiphile promoted the formation of spherical and hexagonal structures, while Pd(II)-coordination promoted the formation of cylindrical and lamellar structures. Importantly, such diverse self-assembly *via* metal-coordination is beyond the conventional concept of the critical packing parameter (CPP), because the CPP does not consider metal–metal interactions. Our methodology could therefore lead to the achievement of novel nanoarchitectonics in materials science with various functions of atomic-level precision.

Author contributions

T. Taira and T. Yanagimoto completed the experiment and analysed the data. T. Taira and T. Imura designed and supervised the project. T. Taira wrote the original draft, and all authors discussed the results.

Conflicts of interest

There are no conflicts to declare.

Acknowledgements

Notes and references

1 J.-M. Lehn, *Proc. Natl. Acad. Sci. U. S. A.*, 2002, **99**, 4763–4768; G. M. Whitesides and B. Grzybowski, *Science*, 2002, **295**, 2418–2421.

2 M. Aono, Y. Bando and K. Ariga, *Adv. Mater.*, 2012, **24**, 150–151; T. Govindaraju and M. B. Avinash, *Nanoscale*, 2012, **4**, 6102–6117; M. B. Avinash, K. Swathi, K. S. Narayan and T. Govindaraju, *ACS Appl. Mater. Interfaces*, 2016, **8**, 8678–8685; M. B. Avinash and T. Govindaraju, *Acc. Chem. Res.*, 2018, **51**, 414–426; K. Ariga, A. Vinu, Y. Yamauchi, Q. Ji and J. P. Hill, *Bull. Chem. Soc. Jpn.*, 2012, **85**, 1–32.

3 P. C. Griffiths, I. A. Fallis, T. Chuenpratoom and R. Watanesk, *Adv. Colloid Interface Sci.*, 2006, **122**, 107–117; P. C. Griffiths, I. A. Fallis, T. Tatchell, L. Bushby and A. Beeby, *Adv. Colloid Interface Sci.*, 2008, **144**, 13–23; P. C. Griffiths, I. A. Fallis, C. James, I. R. Morgan, G. Brett, R. K. Heenan, R. Schweins, I. Gtillo and A. Paul, *Soft Matter*, 2010, **6**, 1981–1989; J. Zhang, X.-G. Meng, X.-C. Zeng and X.-Q. Yu, *Coord. Chem. Rev.*, 2009, **253**, 2166–2177; S. Polarz, S. Landsmann and A. Klaiber, *Angew. Chem., Int. Ed.*, 2014, **53**, 946–954.

4 E. Levin, E. Ivry, C. E. Diesendruck and N. G. Lemcoff, *Chem. Rev.*, 2015, **115**, 4607–4692.

5 T. Taira, T. Yanagimoto, K. Sakai, H. Sakai, A. Endo and T. Imura, *Tetrahedron*, 2016, **72**, 4117–4122.

6 T. Taira, T. Yanagimoto, K. Sakai, H. Sakai, A. Endo and T. Imura, *J. Oleo Sci.*, 2018, **67**, 1107–1115.

7 T. Taira, T. Yanagimoto, T. Fouquet, K. Sakai, H. Sakai and T. Imura, *J. Oleo Sci.*, 2020, **69**, 871–882.

8 J. Lipfert, L. Columbus, V. B. Chu, S. A. Lesley and S. Doniach, *J. Phys. Chem. B*, 2007, **111**, 12427–12438.

9 L. K. Shrestha, S. C. Sharma, T. Sato, O. Glatter and K. Aramaki, *J. Colloid Interface Sci.*, 2007, **316**, 815–824.

10 L. K. Shrestha, R. G. Shrestha, K. Oyama, M. Matsuzawa and K. Aramaki, *J. Oleo Sci.*, 2010, **59**, 339–350.

11 P. de Frémont, R. Singh, E. D. Stevens, J. L. Petersen and S. P. Nolan, *Organometallics*, 2007, **26**, 1376–1385; D. V. Partyka and N. Deligonul, *Inorg. Chem.*, 2009, **48**, 9463–9475.

12 J. C. Garrison, R. S. Simons, J. M. Talley, C. Wesdemiotis, C. A. Tessier and W. J. Youngs, *Organometallics*, 2001, **20**, 1276–1278; H.-L. Su, L. M. Pérez, S.-J. Lee, J. H. Reibenspies, H. S. Bazzi and D. E. Bergbreiter, *Organometallics*, 2012, **31**, 4063–4071; H. M. J. Wang and I. J. B. Lin, *Organometallics*, 1998, **17**, 972–975.

13 J. Chen, Z. Zhang, C. Wang, Z. Gao, Z. Gao and F. Wang, *Chem. Commun.*, 2017, **53**, 11552–11555.

14 P. Pyykkö, *Chem. Rev.*, 1997, **97**, 597–636.

15 K. M. Anderson, A. E. Goeta and J. W. Steed, *Inorg. Chem.*, 2007, **46**, 6444–6451.

16 W. Haiss, N. T. K. Thanh, J. Aveyard and D. G. Ferning, *Anal. Chem.*, 2007, **79**, 4215–4221.

17 J. Vignolle and T. D. Tilley, *Chem. Commun.*, 2009, 7230–7232.

18 O. Glatter, *J. Appl. Crystallogr.*, 1979, **12**, 166–175; L. K. Shrestha, S. C. Sharma, T. Sato, O. Glatter and K. Aramaki, *J. Colloid Interface Sci.*, 2007, **316**, 815–824;

L. K. Shrestha, M. Yamamoto, S. Arima and K. Aramaki, *Langmuir*, 2011, **27**, 2340–2348.

19 A. Picco, M. Kraska, H. Didzoleit, C. Appel, G. Silbestri, O. Azzaroni, B. Stühn and M. Ceolin, *J. Colloid Interface Sci.*, 2014, **436**, 243–250.